Investigation on parameters used in warning systems for rain-induced embankment instability

Chaminda Gallage
School of Urban Development, Faculty of Built Environment & Engineering, Queensland University of Technology (QUT), Brisbane, QLD, Australia
Taro Uchimura
Department of Civil Engineering, University of Tokyo, Tokyo, Japan

ABSTRACT
A number of instrumented laboratory-scale soil embankment slopes were subjected to artificial rainfall until they failed. The factor of safety of the slope based on real-time measurements of pore-water pressure (suction) and laboratory measured soil properties were calculated as the rainfall progressed. Based on the experiment measurements and slope stability analysis, it was observed that slope displacement measurements can be used to warn the slope failure more accurately. Further, moisture content/pore-water pressure measurements near the toe of the slope and the real-time factor of safety can also be used for prediction of rainfall-induced embankment failures with adequate accuracy.

RÉSUMÉ
Un certain nombre de remblais recrées en laboratoire ont été soumis a des précipitations artificielles jusqu'à leur défaillance. Le coefficient de sureté de la pente, basé sur des mesures en temps réel de la pression d'eau interstitielle and des propriétés du sol, a été calculé au fur et a mesure de la progression des précipitations. Sur la base de l'analyse de la stabilité du sol et des mesures calculées, on a pu observer que les mesures de déplacement de la pente peuvent être utilisées pour prévenir la défaillance de ladite pente de façon plus précise. De plus, la teneur en humidité à proximité de la base de la pente ainsi que le facteur de sécurité en temps réel peuvent également être utilisé avec une certaine exactitude pour prédire la défaillance de remblais causée par des précipitations.

1 INTRODUCTION

Embankments are geo-structures that are widely used to support rails and roads. The failure of such structures may lead to large numbers of human casualties. Rainfall has been identified as one of major causes to make embankments unstable and subsequent failures.

The warning against the failure and instability of the embankment slope can save the human casualties by evacuating people living near the slope and stopping the operation of rails or roads supported by the embankments. The most available methods for predicting rain-induced slope instability are based on statistic of past slope failure data and real-time rainfall measuring data. Therefore, these methods often give faulty warnings disrupting human lives and leading to economical lost due to interrupted transportation services. A physically based system would give more accurate warning against failure and instability of the embankments. Further, such a system can also be used to determine when to resume the operation after rainfall once it is suspended due to rainfall-induced instability.

This paper describes results of an instrumented model embankment test subjected to artificial rainfall. Measured pore-water pressure and water content near the toe, surface displacement, and factor of safety are then discussed as possible parameters to be used in physically based warning system against rainfall-induced embankment instability.

2 TEST MATERIAL

Edosaki soil procured from a natural slope in Ibaraki prefecture in Japan was employed in the experimental work of this study. Wet sieving analysis and hydrometer tests were performed on this material as it contains fines (particles finer than 0.075 mm) content of 17.1 %. The grain-size distribution curve of the test material is shown in Figure 1. The specific gravity, maximum void ration, and minimum void ratio of the soil were measured as 2.75, 1.59, and 1.01, respectively. The soil was found to be non-plastic. The optimum gravimetric water content and the maximum dry density of the sand obtained from the standard proctor compaction test were 16.5% and 1.725 g/cm^3 respectively. According to the Unified Soil Classification System, the soil can be classified as silty sand

2.1 Soil Water Characteristic Curve (SWCC)

Figure 2 depicts the soil-water characteristic curve (SWCC) for Edosaki sand obtained in the laboratory using a Tempe pressure cell. Both the drying and the wetting SWCCs were obtained for the test material using a sample with dry density of 1.22 g/cm^3. Model slopeswere constructed using Edosaki sand to achieve dry density of 1.22 g/cm^3.Since the air-entry value of the ceramic disk used in Tempe pressure cell is 300 kPa, the measured SWCCs were restricted to the maximum

suction of 200 kPa. More details about SWCC measurement using Tempe pressure cell is given in Gallage et al. (2010). As shown Figure 2, the laboratory measured SWCC data were fitted using the equation proposed by Fredlund and Xing (1994).

The equation proposed by Fredlund & Xing (1994) is given in Equation [1]

$$\theta(\psi,a,n,m)=C(\psi)\frac{\theta_s}{\left\{\ln\left[e+(\psi/a)^n\right]\right\}^m} \quad [1]$$

where $C(\psi)$ is a correction function defined as

$$C(\psi)=1-\frac{\ln(1+\psi/\psi_r)}{\ln[1+(1000000/\psi_r)}} \quad [2]$$

and θ = Volumetric water content, Ψ = Suction (kPa), Ψ_r = Residual suction, θ_s = Volumetric water content at zero suction, *a,n.m* = Fitting parameters (*a* has the unit of pressure (kPa)).

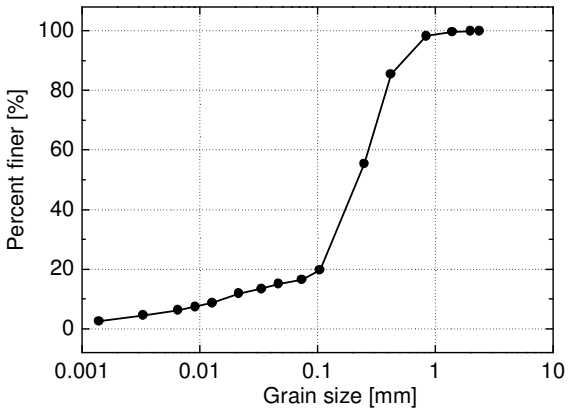

Figure 1. Grain size distribution curve of Edosaki sand

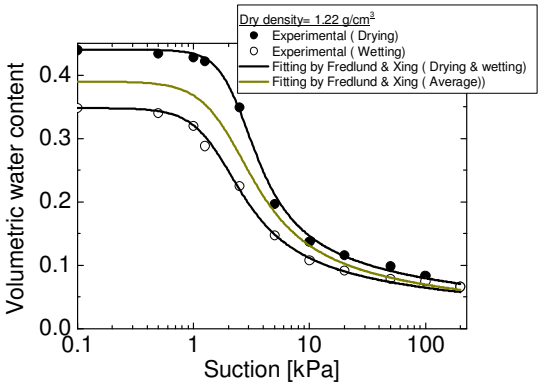

Figure 2. SWCCs of test material

2.2 Unsaturated Permeability

Permeability function of unsaturated soils was measured using a laboratory developed permeameter based steady –state method (Klute, 1965). It was observed that the new apparatus could be used to measure the permeability function of unsaturated soil with adequate accuracy in low suction range (e.g: 0 ~ 8 kPa) following the drying path of SWCC.

Figure 3 shows the variation of measured coefficient of permeability with suction following the drying path of the SWCC. The test was conducted on the dry density of 1.22 g/cm^3 of Edosaki sand. There are some numerical models to predict the unsaturated permeability function using the saturated permeability coefficient and the SWCC. Figure 3 also compares the laboratory measured permeability function with the predictions using the methods proposed by Fredlund (1994), Green & Corey (1971), and Van Genuchten (1980) (all three methods are included in SEEP/W - 2004). It can be observed that the methods proposed by Fredlund and Green & Corey can be used to predict permeability function for the testing material. In this study the method proposed by Fredlund (1994) is used to predict unsaturated permeability function when using SEEP/W for seepage analysis.

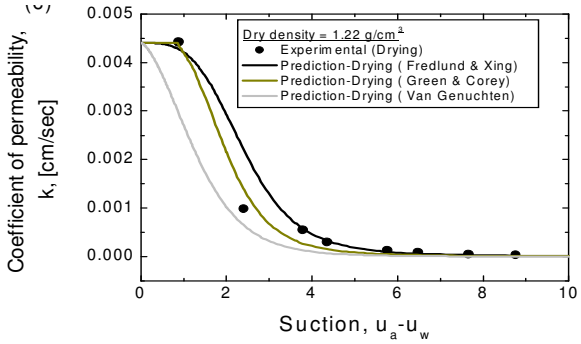

Figure 3. Measured and predicted permeability function of test material

2.3 Unsaturated Shear Strength

Fredlund (1978) proposed an equation (Equation [3]) to interpret the shear strength of unsaturated soils in terms of two stress state variables,

$$\tau=(\sigma_n-u_a)\tan\phi^{'}+c \quad [3]$$

$$c=c^{'}+(u_a-u_w)\tan\phi^b \quad [4]$$

where τ = shear strength of unsaturated soil; c = apparent cohesion; $c^{'}$ = effective cohesion of saturated soil; $\phi^{'}$ = the shearing resistance angle which is assumed to be constant for all values of matric suction and is equal to saturate condition; ϕ^b = the angle of shearing resistance with respect to suction; σ_n = the total normal stress on the plane of failure; u_a = air pressure in the soil mass; u_w = pore water pressure; (u_a-u_w) = the matric

suction of the soil in the failure plane.

In this interpretation, the relationship between τ and (u_a-u_w) is assumed to be linear. However, (Escario & Saez 1986) determined that this relationship is actually non-liear. Later several other researchers observed the non-linear relation between apparent cohesion and matric suction (Fredlund et al. 1987; Wheeler 1991; Ridley 1995; Ridley et al. 1995).

A conventional direct shear apparatus was modified to measure unsaturated shear strength under controlled suction. Figure 4 (a) depicts the variation of the ϕ' with the suction. The ϕ' was obtained from both saturated and unsaturated consolidated drained tests employing the modified direct shear device. The results suggested that the effects of suction on the ϕ' is not significant. However, as shown in Figure 4 (b), the apparent cohesion (c) increases with the suction in the decreasing rate.

For the stability analysis in this study, ϕ^b was obtained assuming linear relationship between the c and the suction for the range of small suction (0 ~ 20 kPa). This seems to be a reasonable assumption for the purpose of the prediction of rain-induced slop instability as slopes become unstable at low suction values. Furthermore, it can be suggested that the use of unsaturated shear strength parameters obtained from the direct shear device may give a conservative solution which is favorable in issuing warnings for the failure of slopes.

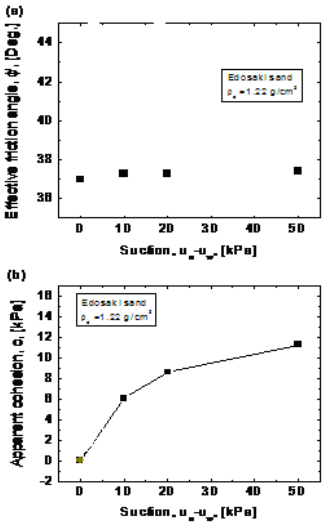

Figure 4. Measured unsaturated shear strength properties of test material

3 MODEL TESTS

In this study, a series of model tests of an instrumented embankment subjected to artificial rainfall was performed with different materials, initial densities, boundary conditions, rainfall intensities and durations, and slope angles. However, the results of a test are discussed in this paper for identifying parameters to be used in a warning system for rain-induced embankment instability.

3.1 Instruments Used

The tank (Figure 5) used in model test has a length of 2.0 m, width of 0.8 m, and a height of 1.0 m. The walls of the tank are made up of steel plates, except for the front side which is made of acrylic glass for easy observation of deformation processes.

ADR (Amplitude Domain Reflectometry) and ECHO types soil moisture sensors were used in the model tests to measure soil moisture content during water infiltration. In order to measure both positive and negative water pressures, KYOWA 05 PMG pressure sensors were modified with a ceramic cup of 100 kPa air-entry value. Figure 6 shows the types of sensors used in the model tests. LVDTs were used to measure the local displacements on the slope surface. Inclinometers installed in the soil measured the sub-soil displacements. Evaflow side spray irrigation tube (hole size, 0.1 mm) was used to simulate rainfall as shown in Figure 5.

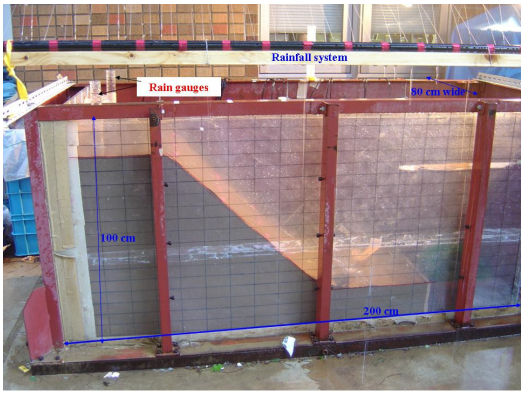

Figure 5. Tank used for model test

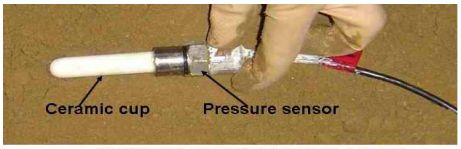

Modified pore water pressure sensor

ADR water content sensor

ECHO water content sensor

Figure 6. Sensors used in model test

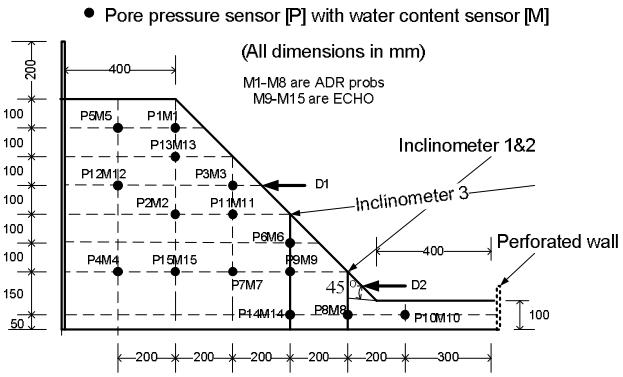

Figure 7. Sensor locations in the model embankment

3.2 Model Preparation

The soil slope shown in Figure 5 was constructed by compacting Edosaki sand with the initial gravimetric water content of 13.5 %. The compaction was performed in order to achieve the dry density of 1.22 g/cm^3. The inclination of the slope was 45^0. 15 pore-water pressure sensors, 15 water content sensors, three inclinometers, and two LVDTs were installed as shown in Figure 7. All the sensors were connected to a data acquisition system for continuous logging of data during the construction of the slope and as well as during rainfall application.

3.3 Rainfall application

Approximately 24 hours after the completion of the construction of the slope, the slope was subjected to a rainfall with an approximate intensity of 40 mm/h. During the rainfall application, it was set to log data for very 2 seconds from all the sensors connected with the logging system.

Evaflow side spray irrigation tube system used in this experiment was able to provide a relatively uniform constant rainfall between 20 mm/hr and 50 mm/hr. It was able to control the rainfall intensity by regulating the pressure of the water supplied to the system. This rainfall system was calibrated to give different rainfall intensities with supplied water pressure. Four measuring cylinders (rain gauges) were used to measure intensity of rainfall; two of them were positioned near the toe and the other two were placed on the top of the embankment. The rainfall intensity mentioned in this study was calculated by averaging the measured rainfall over the entire duration of rainfall and the space. To minimize the possible fluctuation of rainfall intensity with time and space (due to wind), the rainfall was applied in the morning (e.g., 5.30 a.m) in most tests.

3.4 Model Test Results

Figure 8 depicts the monitored time histories of pore-water pressure, volumetric water content, and displacement at various locations within the model slope during the rainfall of 40mm/hr. As shown in Figure 8 (c), the deformation started about 400 sec after the rainfall began and all the deformation transducers responded almost at the same time, suggesting the movement of entire slope. Further, cracks appeared at the crest of the slope (Figure 9) at about 6000 sec after the rainfall began. The formed cracks further widened before local failure was visualized at the toe of the slope (at about 8500 sec after the beginning of rainfall). Once the failure started at the toe, it propagated upward rapidly.

It was interesting to observe that the volumetric water content near the toe (M8 and M10) reached its maximum value (38 % ~ 42 %) well before the deformation started. It was found that 40 % of volumetric water content is approximately equal to degree of saturation of 72 % assuming no changing in dry density of the slope. However, the slope can be densified during construction and rainfall application resulting higher degree of saturation corresponding to 40 % volumetric water content.

The measured pore-water pressures near the toe of the slope (P8 and P10) suggested that the slope began to move as the pore-water pressure near the toe approached zero (full saturation). However, the most part of the slope was remained unsaturated at the beginning and during the movement of the slope. This was observed in most model tests conducted in this study. Therefore, in addition to displacement, it can be concluded that pore-water pressure or degree of saturation measured near the toe of the slope could be a parameter used in warning system of embankment instability.

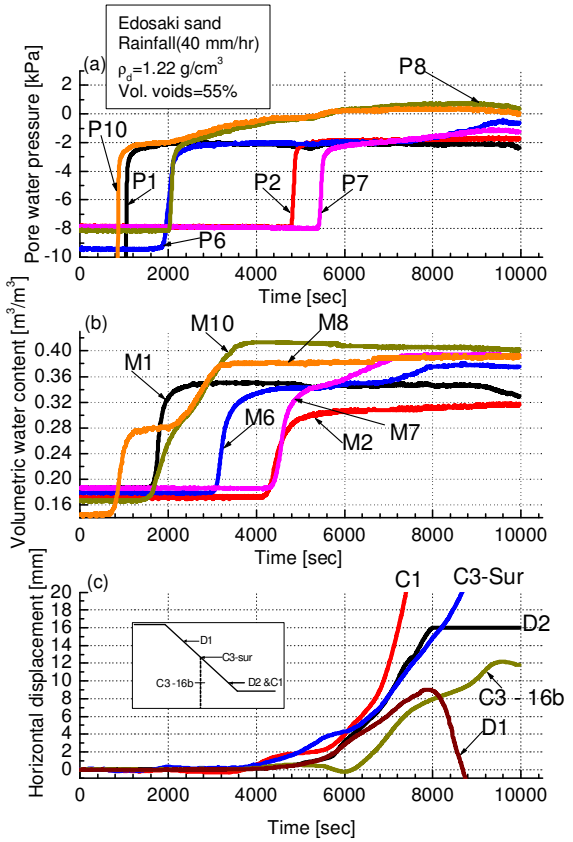

Figure 8. The time histories of measured (a) pore-water pressure, (b) moisture content, (c) soil displacement

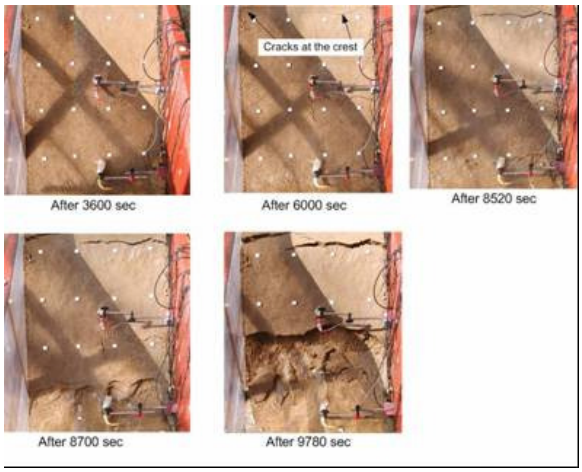

Figure 9. Failure in the model test during the rainfall

4 STABILITY ANALYSIS ON THE MODEL SLOPE

The transient seepage analysis was conducted on the model test using SEEP/W as the rainfall progressed. The pore-water pressure distribution obtained from the seepage analysis was used in stability analysis to determine the factor of safety of the slope as the rainfall progressed.

4.1 Seepage Analysis

FE mesh shown in Figure 10 was used in the numerical seepage analysis of the model test using SEEP/W. AF and FE boundaries were considered as "no-flow" boundaries (Q=0) as no water flow was allowed through these boundaries during the test. Boundary ABCD was defined as a flux boundary where the rainfall intensity (40 mm/hr) was given. Both ABCD and DE were defined as seepage faces in order to allow water to seep out from the model. The initial pore-water pressure at each node was given by defining the water table according to the initial pore-water pressure readings of P1, P2, and P8.

Laboratory measured wetting SWCC and saturated permeability was given to the SEEP/W to generate the permeability function using the method proposed by Fredlund (1994).

The seepage analysis was conducted for 9500 sec with incremental time of 5 sec. Once the analysis was completed, measured and simulated pore-water pressure time histories were compared at some selected points (P1, P2, P7, and P8) in the slope. As shown in Figure 11, a reasonable agreement between measured and simulated pore-water pressures was observed.

4.2 Stability Analysis

The geometry shown in Figure 12 was used for numerical stability analysis in SLOPE/W. ABC and DEF were defined as entry and exit surfaces, respectively, for the trial slip surfaces. The laboratory measured saturated/unsaturated shear strength properties of Edosaki sand were for the analysis. Using the pore-water pressure obtained from numerical seepage analysis, the stability analysis was performed by selecting the GLE (general limit equilibrium) method. As shown in Figure 13, the FOS (Factor of Safety) decreases with time as the rainfall proceeds. It can be seen that the slope starts to move when the FOS goes below unity.

Figure 14 compares the critical slip surface that was obtained from stability analysis when the FOS is just below unity with the slip surface observed by the movement of markers. These two slip surfaces seem to agree reasonably well.

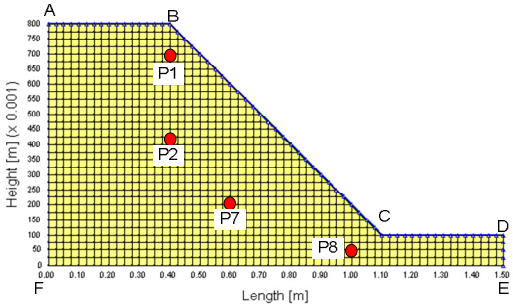

Figure 10. FE mesh used in SEEP/W analysis

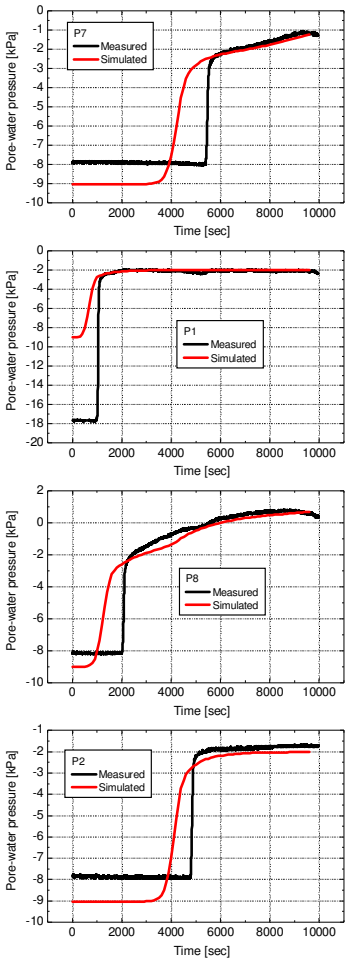

Figure 11. Comparison of measured and predicted pore-water pressures at some selected locations in the model slope

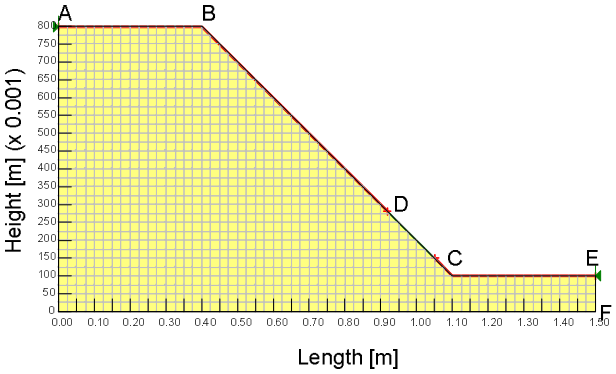

Figure 12. Geometry used for stability analysis

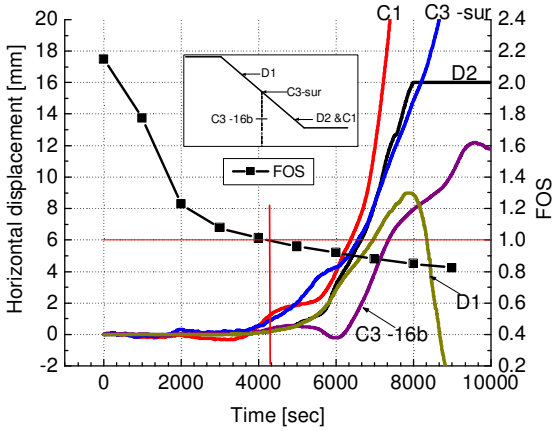

Figure 13. Decrease in FOS and increase in soil displacement as rainfall proceeds

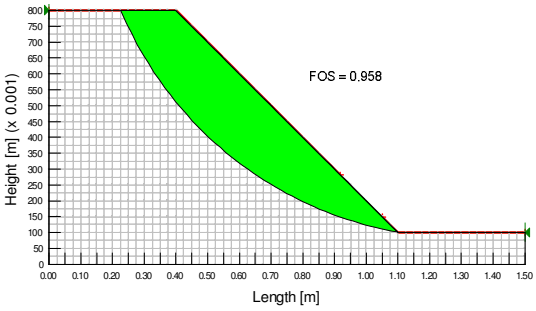

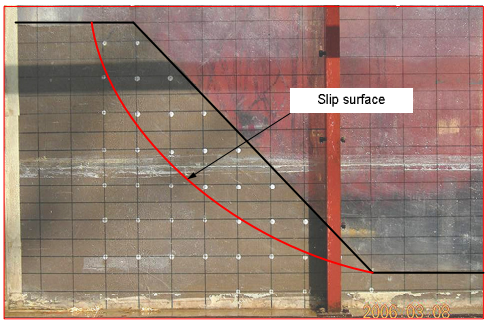

Figure 14: Comparison of observed slip surface with one obtained by stability analysis

5 DISCUSSION ON EXPERIMENTAL AND ANLYTICAL RESULTS

It can be seen from the model test experiment that the cracks appeared at the crest at about 6000 sec after the beginning of the rainfall. The local failure began at the toe after 8700 sec and it propagated rapidly upward and complete collapse of the slope occurred at about 9800 sec after the beginning of rainfall.

As shown in Figure 13, the slope began to move at about 4000 sec after the beginning of rainfall which is about 2000 sec before the cracks appeared at the crest. It implies that real-time monitoring of slope movement can be used to warn the slope failure effectively. Further, degree of saturation (pore-water pressure and/or water contents) measured at the toe (Figure 8a & 8b) can also be used for prediction of slope failures. The warning methods based on these parameters can be used to minimise the casualties by relocating people living near the slope. However, the warning based on these parameters would not be sufficient to safely suspend the transportation services supported by the embankment. As shown in Figure 13, the FOS of the slope give an early indication about the stability of the slope and therefore criteria based on FOS of the slope can be used for safe suspension of the operation. Further, the FOS based criteria can also be used to resume the operation after rainfall.

The author has conducted about 16 model tests, varying slope angle, materials, soil density, rainfall intensity to further investigate the effective your of the real-time calculated FOS for safe use of embankment for during and after heavy rainfall events. The results will be published in future. Further, it is intended to investigate the displacement and degree of saturation (pore-water pressure and/or water content) near the toe to predict the impeding failure of the slope due to rainfall.

6 CONCLUSIONS

The following conclusions can be derived from the study described in this paper.

- The effective friction angle of the soil may not depend on suction. However, the apparent cohesion increases at a decreasing rate as the suction increases.
- The failure of the model embankment may occur with the saturation of the area near the toe of the slope.
- Degree of saturation near the toe of the slope and initial surface displacement in the slope can be used to predict and warn the impeding failure of the slope.
- The assessment of real-time FOS of the embankment during rainfall could help in effective management of services (transportation) supported by an embankment.
- To develop physically based warning system against rain-induced embankments/slopes

failures, the real-time monitoring of surface displacement near the toe and the degree of saturation (pore-water pressure or/and water content) near the toe of the slope could be necessary.

ACKNOWLEDGEMENTS

The authors gratefully acknowledge the Promotion Fundamental Transport Research from Japan Railway Construction, Transport and Technology Agency (JRTT) for the financial support for this study.

REFERENCES

Escario, V., and Saez, J. 1986. The shear strength of partly saturated soils, *Geotechnique,* 36: 453-456.

Fredlund, D. G., and Xing, A. 1994. Equation for the soil-water characteristic curve, *Canadian Geotechnical Journal,* 31: 521-532.

Fredlund, D. G., Xing, A., and Huang, S. 1994. Prediction of the permeability function for unsaturated soils using the soil-water characteristic curve, Canadian Geotechnical Journal, 31: 533-546.

Fredlund, D. G., Rahardjo, H., and Gan, J. K. M. 1987. Non linearity of strength envelope for unsaturated soils, *Proceedings of the 6th International Conference on Expansive Soils*, New Delhi, India, 49-54.

Fredlund, D. G., Morgenstern, N. R., and Widger, R. A. 1978. The shear strength of unsaturated soils, *Canadian Geotechnical Journal*, 15: 313-321.

Gallage, C. P. K., and Uchimura, T. 2010. Effect of dry density and grain size distribution of soil-water characteristic curve of sandy soils, *Soils and Foundations*, 50(1): 161-172.

Green, R. E., and Corey, J. C. 1971. Calculation of hydraulic conductivity: A further evaluation of some predictive methods, *Soil Science Society of America Proceedings*, 35: 3-8.

GEO-SLOPE. 2004. SEEP/W, GEO-SLOPE International Ltd., Calgary, Alberta, Canada.

GEO-SLOPE. 2004. SLOPE/W, GEO-SLOPE International Ltd., Calgary, Alberta, Canada.

Klute, A. 1965. Laboratory measurement of hydraulic conductivity of Unsaturated soil, *in methods of soil analysis,*Mono. 9, Part 1, Amer. Soc. Of Agronomy, Madison, WI, 253-261.

Ridley, A. M. 1995. Strength-suction-moisture content relationships for Kaolin under normal atmospheric conditions, *UNSAT*, Paris, 2: 645-651.

Van Genuchten, M. T. 1980. A closed-form equation for predicting the hydraulic conductivity of unsaturated soils, *Soil Science Society of American Journal*, 44: 892-898.

Wheeler, S. J. 1991. An alternative framework for unsaturated soil behavior, Technical note, *Geotechnique*, 45(2): 257-261.